

Discovery prospects of a vectorlike top partner decaying to a singlet boson

Akanksha Bhardwaj,^{1,*} Kartik Bhide^{2,†}, Tanumoy Mandal^{2,‡}, Subhadip Mitra^{3,§}, and Cyrin Neeraj^{3,||}

¹*School of Physics & Astronomy, University of Glasgow, Glasgow G12 8QQ, United Kingdom*

²*Indian Institute of Science Education and Research Thiruvananthapuram, Vithura, Kerala 695 551, India*

³*Center for Computational Natural Sciences and Bioinformatics,
International Institute of Information Technology, Hyderabad 500 032, India*



(Received 31 May 2022; accepted 26 September 2022; published 24 October 2022)

The possibility of a vectorlike top partner decaying to a new colorless weak-singlet scalar or pseudoscalar has attracted some attention in the literature. We investigate the production of a weak-singlet charge- $2/3$ T quark that can decay to a spinless boson (Φ) and a top quark at the LHC. Earlier [A. Bhardwaj *et al.*, Roadmap to explore vectorlike quarks decaying to a new scalar or pseudoscalar, [arXiv:2203.13753](https://arxiv.org/abs/2203.13753).], we showed that in a large part of the parameter space, the $T \rightarrow t\Phi$ and the loop-induced $\Phi \rightarrow gg$ decays become the dominant decay modes for these particles. Here, we investigate the discovery prospects of the T quark in this region through the above decays. In particular, we focus on the $pp \rightarrow TT \rightarrow (t\Phi)(t\Phi) \rightarrow (t(gg))(t(gg))$ channel. Separating this signal from the huge Standard Model background is a challenging task, forcing us to employ a multivariate machine-learning technique. We find that the above channel can be a discovery channel of the top partner in the large part of the parameter space where the above decay chain dominates. Our analysis is largely model independent, and hence our results would be useful in a broad class of new physics models.

DOI: [10.1103/PhysRevD.106.075024](https://doi.org/10.1103/PhysRevD.106.075024)

I. INTRODUCTION

Various beyond the Standard Model (BSM) scenarios contain heavy companions of the Higgs and the top in the spectrum. For example, we can consider those addressing the hierarchy problem like the partial compositeness models [1–7], extra-dimensional models [8–13], Little-Higgs models [14–17], etc. Generally, in these models, the top partners (T) are vectorlike and decay to a third-generation quark plus a Higgs or a Standard Model (SM) vector boson, W/Z . Recently, however, a new exotic decay possibility of T has attracted considerable attention in the literature [18–42] where a T quark decays to the top quark along with a scalar (ϕ) or pseudoscalar (η) that is SM singlet. This is possible if the singlet boson is lighter than the top partner at least by m_t .

In an earlier paper [43], we explored this possibility. If such a new decay of T exists, the current exclusion limit on T from the direct LHC searches (that assume the T quark

decays to SM-only final states) relaxes significantly. In that paper, based on the weak representation of the vectorlike quarks, we obtained some simple generic phenomenological models containing a singlet $\Phi = \{\phi, \eta\}$ and either a weak-singlet vectorlike quark (VLQ) or a $(T B)^T$ doublet. For these generic models, we recast the current exclusion limits on T . In the singlet T model, Φ gains coupling with the top quark and the gauge bosons through $T \leftrightarrow t$ mixing after electroweak symmetry breaking (EWSB). This leads to a host of new search possibilities to probe the $T + \Phi$ setup at the LHC.

In that paper, we listed various search channels that can probe different regions of the parameter space. Prospects of some of these channels at the high luminosity LHC (HL-LHC) have been studied in the literature. For example, Ref. [29] examines the prospects of an unusual channel containing six top quarks in the final states. The six top quarks arise from the pair production of T as

$$pp \rightarrow T\bar{T} \rightarrow (t\Phi)(\bar{t}\Phi) \rightarrow (t(\bar{t}))(\bar{t}(\bar{t})). \quad (1)$$

The process is kinematically viable only if $M_\Phi > 2m_t$ and $M_T > M_\Phi + m_t$. Reference [33] has a detailed analysis of the pair production of the singlet T quark when the top partner decays to a photon pair plus a top quark via Φ : $T \rightarrow t\Phi \rightarrow t\gamma\gamma$. This channel is a clean probe of the new decay mode of $T \rightarrow t\Phi$ but suffers from low $\Phi \rightarrow \gamma\gamma$ branching.

*akanksha.bhardwaj@glasgow.ac.uk

†kartikdbhide17@iisertvm.ac.in

‡tanumoy@iisertvm.ac.in

§subhadip.mitra@iiit.ac.in

||cyrin.neeraj@research.iiit.ac.in

Published by the American Physical Society under the terms of the [Creative Commons Attribution 4.0 International license](https://creativecommons.org/licenses/by/4.0/). Further distribution of this work must maintain attribution to the author(s) and the published article's title, journal citation, and DOI. Funded by SCOAP³.

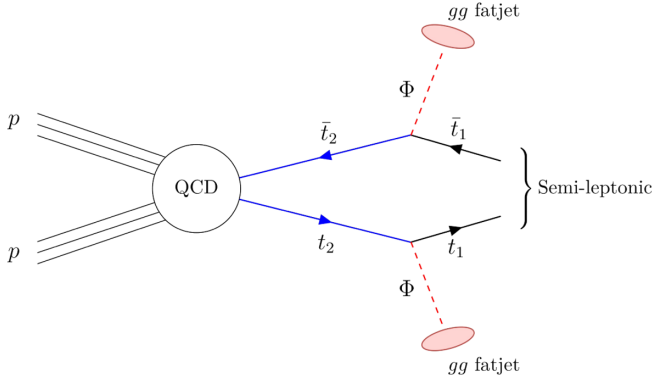


FIG. 1. The signal topology.

We made two interesting observations in Ref. [43]. First, even though Φ decays to a $t\bar{t}$ pair through a tree-level process beyond the mass threshold, it can also decay to a couple of gluons mainly via a T loop. Second, the part of parameter space where the loop-mediated Φ decay dominates is large, and the corresponding parameters (i.e., couplings) are not fine-tuned. Hence, in a large part of the parameter space, the dominant decay of the T quark is $T \rightarrow (t\Phi) \rightarrow t(gg)$. In other words, the pair production of T would have the following signature in a large region of the parameter space:

$$pp \rightarrow T\bar{T} \rightarrow (t\Phi)(\bar{t}\Phi) \rightarrow (t(gg))(\bar{t}(gg)). \quad (2)$$

(It is not difficult to achieve a large $T \rightarrow t\Phi$ branching since the coupling controlling the decay is independent of the small $t \leftrightarrow T$ mixing angle.) Therefore, to probe that parameter region, one has to rely on the above channel (see Fig. 1). However, since the SM background is huge for this channel, isolating this signal is arduous. In this paper, we take up this task and show that a large parameter region can be discovered through this channel at the HL-LHC with the help of jet substructure and multivariate machine-learning techniques.

This paper is organized as follows: In Sec. II we describe the singlet T model from Ref. [43] and the constraints on its parameters, in Sec. III we describe our analysis from event generation to multivariate analysis and present the results, and conclude in Sec. IV.

II. THE SINGLET T MODEL

From Ref. [43], we select the simple extension of the SM containing a TeV-range weak-singlet VLQ, $T \equiv (\mathbf{3}, \mathbf{1}, 2/3)$ and a lighter SM-singlet scalar or pseudoscalar. We can write the top-sector mass terms in the interaction basis as (more details are given in the Appendix):

$$\mathcal{L} \supset (\bar{t}_L \quad \bar{T}_L) \begin{pmatrix} m_t & \mu_1 \\ 0 & M_T \end{pmatrix} \begin{pmatrix} t_R \\ T_R \end{pmatrix} + \text{H.c.} \quad (3)$$

Throughout the paper, we use similar notations as Ref. [43]. We diagonalize the mass matrix by biorthogonal rotations through two mixing angles θ_L and θ_R ,

$$\begin{pmatrix} t_{L/R} \\ T_{L/R} \end{pmatrix} = \begin{pmatrix} c_{L/R} & s_{L/R} \\ -s_{L/R} & c_{L/R} \end{pmatrix} \begin{pmatrix} t_{1L/R} \\ t_{2L/R} \end{pmatrix}, \quad (4)$$

where $s_P = \sin \theta_P$ and $c_P = \cos \theta_P$ for the two chirality projections, and t_1 and t_2 are the mass eigenstates. We identify the t_1 quark with the physical top quark (we refer to it just as t for simplicity). For a small $t \leftrightarrow T$ overlap, t_2 is mostly the T quark. The top partner can decay to the SM quarks along with a W , Z , or h boson. With the introduction of Φ , a new decay mode opens up: $t_2 \rightarrow t\Phi$. For this new decay, the relevant terms in the Lagrangian are

$$\mathcal{L}_{\text{int}}^T = -\lambda_\Phi^a \Phi \bar{T}_L \Gamma T_R - \lambda_\Phi^b \Phi \bar{T}_L \Gamma t_R + \text{H.c.}, \quad (5)$$

where $\Gamma = \{1, i\gamma_5\}$ for $\Phi = \{\phi, \eta\}$. Expanding t and T in terms of t_1 and t_2 gives

$$\mathcal{L} \supset -\lambda_\Phi^a \Phi (c_L \bar{t}_{2L} - s_L \bar{t}_{1L}) \Gamma (c_R t_{2R} - s_R t_{1R}) - \lambda_\Phi^b \Phi (c_L \bar{t}_{2L} - s_L \bar{t}_{1L}) \Gamma (c_R t_{1R} + s_R t_{2R}) + \text{H.c.} \quad (6)$$

Before EWSB, Φ essentially couples only with the top partner. When the symmetry breaks, T mixes with the SM top quark, and through it, Φ couples to the top quark. It also has loop-mediated effective couplings to the SM gauge bosons. Thus it can decay to $t\bar{t}$, gg , $\gamma\gamma$, $Z\gamma$, ZZ final states (when kinematically allowed). The expressions for the decay widths in the dominant decay modes of Φ are available in Ref. [43]. As explained in the Introduction, in this paper, we consider the Φ boson dominantly decaying to a pair of gluons.

Exclusion bounds on T.—The VLQ searches at the LHC assume that a top partner can only decay to a third-generation quark and a SM boson. Depending on the weak representations of T and branching ratios (BRs) in the conventional decay modes, the limits from the LHC searches vary from 1.29–1.57 TeV [44–47]. Currently, the mass limit on a weak-singlet T stands at 1.29 TeV [45]. With the introduction of the singlet Φ , the assumption on the Φ decays changes to

$$\beta_{bW} + \beta_{tZ} + \beta_{th} = 1 - \beta_{t\Phi}, \quad (7)$$

where β_X is the BR for the $t_2 \rightarrow X$ decay. For a heavy t_2 , $\beta_{bW} \approx 2\beta_{tZ} \approx 2\beta_{th}$ in the singlet T model. With this, one can recast the bounds from the latest searches [44,45,48] in each final state and pick the strongest limit. In Fig. 2, we show the recast mass limits on T in the presence of the new decay mode from Ref. [43].

Bounds on Φ .—In this paper, we are primarily concerned about the BR of the $\Phi \rightarrow gg$ decay. This decay is mediated by t and t_2 loops in the physical basis. As mentioned earlier,

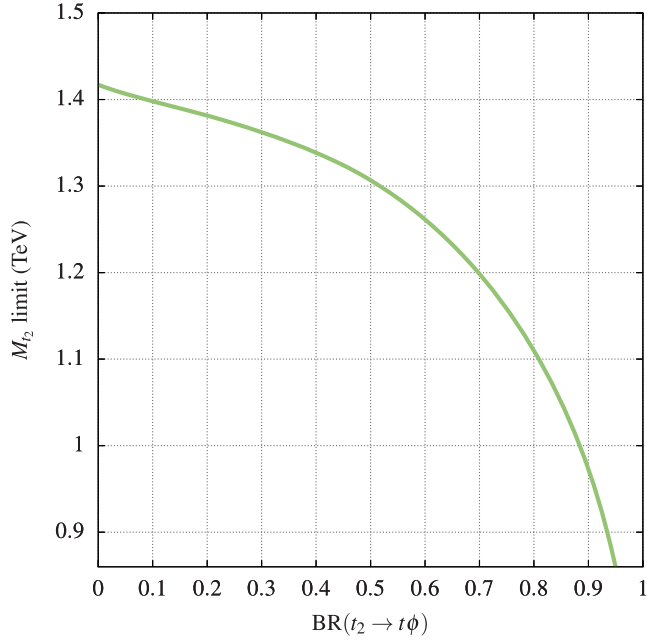


FIG. 2. LHC exclusion limits on t_2 in the singlet T model as a function of the branching ratio in the new decay mode.

this decay is dominant over a large region of phase space allowed by the LHC data.¹ In other words, we can choose a value of $\text{BR}(\Phi \rightarrow gg)$ and find suitable parameter combination(s) from the allowed region without any fine-tuning (for both ϕ and η).

III. COLLIDER ANALYSIS

We use `MadGraph5_aMC@NLO`v3.2.0 [50] to generate the signal and background events at the 14 TeV LHC with CTEQ6L1 parton distribution functions [51], PYTHIA8v8.2 [52] for parton showering and hadronization, and DELPHESv3.5.0 [53] to simulate the detector environment. We use the default CMS card with jets of radius $R = 0.4$ clustered with the anti- k_t algorithm [54] in `FastJet` v3.3.4 [55]. For the higher-order effects, we multiply the leading order cross sections with the highest order K factors available in the literature. For the signal, we estimate the next-to-next-to-leading order (NNLO) K factor as 1.43 in the mass range of interest using the HATHOR package [56].

A. Pair production: Signal topology and selection criteria

The signal process is $pp \rightarrow t_2 \bar{t}_2 \rightarrow \Phi t \Phi \bar{t}$, with each Φ decaying to a couple of gluons and one of the top quarks decaying leptonically and the other, hadronically. For simulating the signal events, we set $\text{BR}(T \rightarrow t\Phi) = \text{BR}(\Phi \rightarrow gg) = 1$. For our analysis, we scan over the mass

ranges $M_{t_2} \in [1.0, 1.7]$ TeV in steps of 100 and $M_\Phi \in [150, 550]$ GeV in steps of 50 GeV. For each mass point in the scan, we choose the parameters such that the narrow-width approximation is valid for both t_2 and Φ . So, from here on, we treat the BRs as free parameters (rather than the couplings) as we are interested in the decays. This also makes our results interpretable in terms of both ϕ and η , even though we only use the scalar ϕ to generate the signals for our analysis. When $M_{t_2} \gg M_\Phi$, the singlet produced from a t_2 decay would be boosted and produce a fatjet. Based on the signal topology (one lepton, two b jets, two Φ jets) we design the following selection criteria:

- (1) *Exactly one lepton in the event (either e or μ) with $p_T > 10$ GeV and $|\eta| < 2.5$.* To be accepted as a lepton, the separation between a lepton candidate (identified from the tracks) and its nearest AK4 jet² should be greater than $\Delta R = 0.4$.
- (2) *The scalar sum of the p_T 's of the AK4 jets, $H_T > 900$ GeV.*
- (3) *At least two b -tagged jets in the event, where b tagging is done with the default Delphes module [57].* We compare the efficiency of the default Delphes module with the DeepCSV algorithm [58] at the medium working point and find that the tagging efficiencies of the two algorithms in p_T range of our interest are comparable. We call the leading and subleading p_T b jets as b_1 and b_2 , respectively.
- (4) *At least two fatjets in the event.* The candidate fatjets are clustered from the calorimeter towers with the Cambridge-Aachen clustering algorithm [59] and have $R = 1.2$ and $p_T > 300$ GeV. The candidates are then groomed with the SoftDrop [60] algorithm for $z_{\text{cut}} = 0.1$ and $\beta = 0.2$. If a candidate fatjet has at least three constituent hadrons needed to compute the three-point energy correlation functions, it is accepted as a fatjet. We denote the leading and subleading p_T fatjets as J_1 and J_2 , respectively.

A summary of the cross sections, selection efficiencies and expected number of events at 3 ab^{-1} for the signal is shown in Fig. 3.

The efficiency trends seen in Fig. 3(a) can be explained by the boost of the final state. We see an increase followed by a decrease in selection efficiency for a fixed M_Φ . This is the result of an interplay between selection criteria: as M_{t_2} increases, the H_T cut becomes more efficient, but the lepton-number and b -tagging cuts worsen due to poor isolation and reduction in efficiency in the boosted regime. In contrast, for a fixed M_{t_2} , the selection efficiency monotonically increases. As M_Φ increases, the boost available to the top quark reduces, so the b jet is easily tagged and the lepton is more isolated. While a slight reduction in the efficiency of the fatjet cut is seen with

¹In Ref. [43], we have put bounds on the Φgg coupling from the ATLAS resonance search data in the diphoton mode [49].

²AK4 jets are clustered with the anti- k_T algorithm [54] with radius $R = 0.4$.

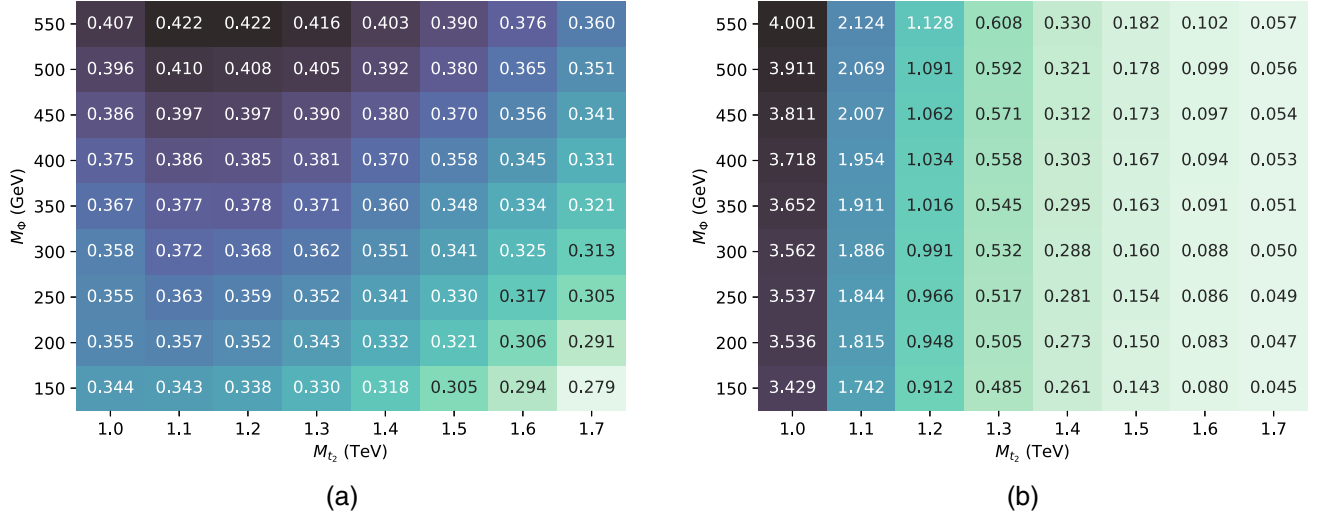


FIG. 3. (a) Selection efficiency for the signal process and (b) effective cross section in fb for the signal process, i.e., $\sigma_{\text{gen}} \times \epsilon \times K$ where σ_{gen} refers to the leading order (generation-level) cross section, ϵ is the selection efficiency and K is the K factor.

increasing M_Φ (due to subjects not being fully resolved in a large- R jet as a consequence of the high mass scalar having lower boost), the overall increase in selection efficiency is governed by the improvement in b tagging.

B. Background processes

Based on the selection criteria, the significant background processes we consider are the semileptonic and leptonic $t\bar{t}$ production, W + jets, single top production via tj and tW processes, and $t\bar{t}X$ production where $X = \{W, Z, H\}$. Of these, the semileptonic $t\bar{t}$ process is the most dominant, followed by the sizable contributions from the W + jets, leptonic $t\bar{t}$, and single top processes. In order to reduce computation time during the background event generation, we employ a strong generation-level cut: $H_T > 500$ GeV. After passing through

the selection cuts, the contribution of the processes like Z + jets, diboson and triboson productions become negligible. The background cross sections, selection efficiencies and expected number of events at 3 ab^{-1} are shown in Table I.

C. Multivariate analysis

We perform a multivariate signal-vs-background discrimination analysis with the boosted decision tree (BDT) algorithm.

Choice of the input features.—There are six physical objects from which we can extract information, namely the lepton, the missing energy, the two leading b -tagged jets and the two leading fatjets. To determine the best features as inputs to the BDT, we start with a large set split into some groups:

TABLE I. Selection efficiency and the expected number of events at 3 ab^{-1} for the background processes. Here σ_{gen} refers to the leading order (generation-level) cross section after the $H_T > 500$ GeV cut. The subscripts l, h refer to the leptonic and hadronic decay modes. The additional jets (in parentheses) indicate the number of matched hard jets, where the jet-parton shower matching is done using the MLM prescription [61].

Process	Selection cut efficiency (ϵ)	Estimated K factor	Effective cross section	
			$\sigma_{\text{eff}} = \sigma_{\text{gen}} \times \epsilon \times K$ (fb)	Events at 3 ab^{-1} $\sigma_{\text{eff}} \times \mathcal{L}$
$t_l \bar{t}_h (+2j)$	0.028759	1.783 (N ³ LO) [62]	838.31	2, 514, 940
$W_l (+2j)$	0.003657	1.189 (NLO) [63]	57.41	172, 222
$t_l \bar{t}_l (+2j)$	0.014806	1.783 (N ³ LO) [62]	29.31	87, 918
$t_l + j (+2j)$	0.018136	1.175 (N ² LO) [64]	18.01	54, 027
1 lepton $tW (+2j)$	0.018806	1.333 (aN ² LO) [64]	12.58	37, 747
1 lepton $t\bar{t}W (+j)$	0.027047	1.572 (NLO + N ² LL) [65]	6.14	18, 411
$t_l \bar{t}_h H_b (+j)$	0.030843	1.410 (NLO + N ² LL) [65]	4.37	13, 125
$t_l \bar{t}_h Z_h (+j)$	0.023209	1.662 (NLO) [66]	3.53	10, 598
				2, 908, 998

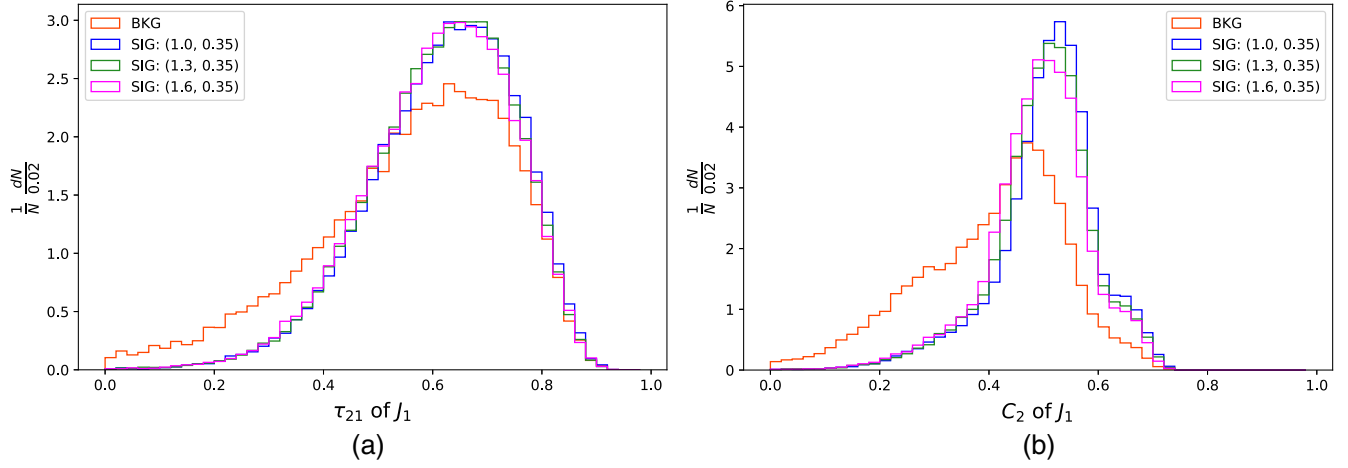


FIG. 4. The features (a) τ_{21} and (b) C_2 calculated for the leading p_T fatjet for different (m_{t_2}, m_ϕ) mass points.

- (1) *Measure of the physical objects:* the number of b -tagged jets, fatjets, and the number of jets with p_T over 20, 40, 50 and 60 GeV. We consider these jet-number features so that the high p_T jets from the Φ decay are captured. This group also includes the H_T feature.
- (2) *Basic kinematic variables:* This group includes p_T , η , and Φ of the six objects considered. We also include the energy E of the visible five objects.
- (3) *Separation variables:* We consider $\Delta\eta$, $\Delta\phi$ and $\Delta R = (\Delta\eta^2 + \Delta\phi^2)^{1/2}$ among the six objects. In total, there are $3 \times {}^6C_2 = 45$ features in this group.
- (4) *Fatjet features:* For the first two leading p_T fatjets, we consider their masses and the number of constituents. Additionally, we include the well-known jet substructure features of the two fatjets, namely NSubjettiness [67] τ_1 , τ_2 , τ_3 , τ_{21} and τ_{32} with $\beta = 0.5$ and the energy correlation function [68] features ECF_1 , ECF_2 , ECF_3 and C_2 with $\beta = 0.2$.
- (5) *Reconstructed T mass:* One can reconstruct the transverse mass of T through the semileptonic decay products as $M_{t_2}^T = m(l\nu bJ)$ if one assigns the missing energy to the neutrino. We calculate four such reconstructed masses for the two b -tagged jets and two fatjets and choose the ones with the minimum and maximum masses.

By looking at the above features for the generated signal and background events, we narrow down the list by discarding objects with less than 1% method-unspecific separation, defined in Ref. [69] as

$$\langle S^2 \rangle = \frac{1}{2} \int dy \frac{(\hat{y}_S(y) - \hat{y}_B(y))^2}{\hat{y}_S(y) + \hat{y}_B(y)}, \quad (8)$$

where \hat{y}_S and \hat{y}_B are the probability density functions of the signal and background respectively for a particular feature y . This quantity is equal to zero for identical signal and

background shapes and 1 for shapes with no overlap. Naturally, features with higher method-unspecific separation are better at discriminating between signal and background events. We also reject features like (most of) the separation variables that are highly correlated with others or do not perform well for different BDT parameter settings. A large number of basic kinematic features and the reconstructed masses are also discarded for the same reasons. Among the measures of physical objects, we retain H_T , the number of jets with $p_T > 50$ GeV (since this one has the best separation compared to the other jet count features) and the number of fatjets.

In the signal, we have two boosted Φ jets that are fatjets basically made up of two gluons. Simple variables such as N_{consti} , i.e., the number of (charged) hadrons in the fatjet, are known to be good discriminators between q - and g -initiated jets [70]. However, since it is highly correlated with the fatjet mass, we do not consider it. The traditional observables like τ_{21} and C_2 hint at the two-pronged nature of the signal fatjets but similar behavior is also seen in the background fatjets since the dominant semileptonic $t\bar{t}$ background has both a boosted W jet and a three-pronged t jet. As a result, the distributions of these observables show little separation between the signal and background (see Fig. 4). In addition, we find that the simpler observables $\tau_{1,2,3}$ and $ECF_{1,2,3}$ show a slight separation but are correlated with each other and with the fatjet masses and p_T 's. Hence, we do not include any jet substructure observables in our analysis.

The final list.—The final list of features chosen as inputs to the boosted decision tree algorithm are³

- (i) H_T , the scalar sum of p_T 's of all final state hadrons.

³During preliminary analysis, we found the Lund Jet Plane to be a promising tool in tagging the gg fatjets, similar to the $H \rightarrow gg$ tagging done in Ref. [71]. However, it requires complex neural network machinery beyond the scope of this paper.

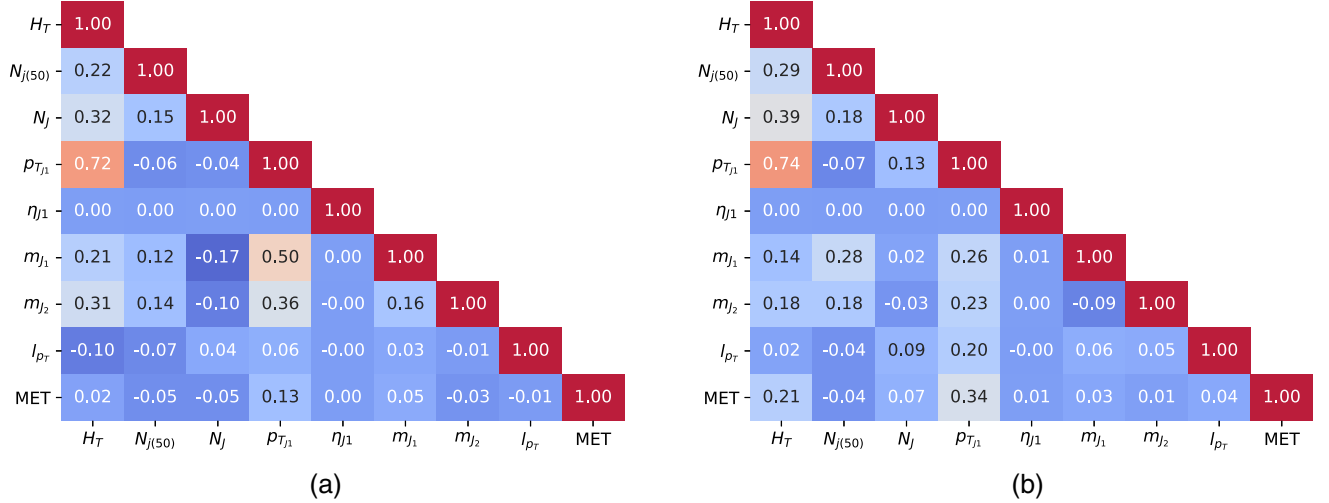


FIG. 5. Linear correlation coefficients for (a) signal and (b) background between the inputs chosen for multivariate analysis at the benchmark mass point. Note that the scale goes from +1 to -0.2 .

- (ii) $N_{j(50)}$ and N_j , the number of AK4 jets with $p_T > 50$ GeV and the number of fatjets respectively.
- (iii) m_{j_1} and m_{j_2} , the masses of the leading and sub-leading fatjets respectively.
- (iv) p_{T_ℓ} and MET, the p_T of the lepton and the transverse missing energy respectively.
- (v) $p_{T_{j_1}}$ and η_{j_1} , the p_T and η coordinate of the leading fatjet respectively.

In Fig. 5, we show the linear correlation coefficients between the input features, defined as

$$\rho(X, Y) = \frac{\langle XY \rangle - \langle X \rangle \langle Y \rangle}{\sigma_X \sigma_Y},$$

where $\langle A \rangle$ and σ_A denote the expectation value and standard deviation respectively for a one-dimensional dataset A .

We see some positive correlation between $\{H_T, p_{T_{j_1}}\}$ for both the signal and background. However, we retain both since H_T is our highest performing variable and $p_{T_{j_1}}$ is a good low-level fatjet feature. We also see some positive correlation between $\{p_{T_{j_1}}, m_{j_1}\}$ only for the signal. Since this correlation is not present for the background, we retain m_{j_1} in our analysis.

We show the input feature distributions for $M_\Phi = 150$ and 450 GeV in Figs. 6 and 7, respectively. In these plots, the background distributions are obtained by a weighted sum of the separate processes:

$$H = \frac{\sum_i h_i w_i}{\sum_i w_i}, \quad (9)$$

where $w_i = N_{\text{exp}}/N_{\text{gen}}$ (N_{exp} and N_{gen} are the expected number of events at 3 ab^{-1} and the number of generated events passing the selection criteria, respectively). The

variable H_T is driven by the mass of t_2 —a heavier t_2 imparts more momentum to the AK4 jets and consequently pushes H_T to higher values. A heavier Φ takes a larger fraction of the momentum of the parent t_2 , leaving a smaller budget for the top quark, and as a consequence, the lepton and neutrino from the top decay are less boosted. This can be seen in the distributions for p_{T_ℓ} and MET as they are slightly pushed towards the lower values for $M_\Phi = 450$ GeV than the $M_\Phi = 150$ GeV case. The η_{j_1} and $p_{T_{j_1}}$ features are more or less similar for the two Φ masses as they merely describe the kinematics of the leading fatjet in the event, be it a top jet or a gg fatjet from a Φ .

While most of the feature distributions look similar for $M_\Phi = 150$ GeV and $M_\Phi = 450$ GeV, some of them do show differences. Since the Φ 's originate in t_2 decays, for a fixed M_{t_2} , a heavier Φ is less boosted than a lighter one. As a result, the two subjets from Φ are more separated for heavy scalars, leading to a shift in the number of AK4 jets and a lower clustering efficiency for $R = 1.2$ fatjets. This in turn affects N_j , m_{j_1} and m_{j_2} (see Fig. 7).

D. BDT results

We optimize the statistical significance of the signal in the BDT analysis. In the absence of any systematic uncertainty, the signal significance over the background can be estimated by the approximate Poisson significance for the Asimov dataset:

$$\mathcal{Z} = \sqrt{2(N_S + N_B) \ln \left(1 + \frac{N_S}{N_B} \right) - 2N_S}, \quad (10)$$

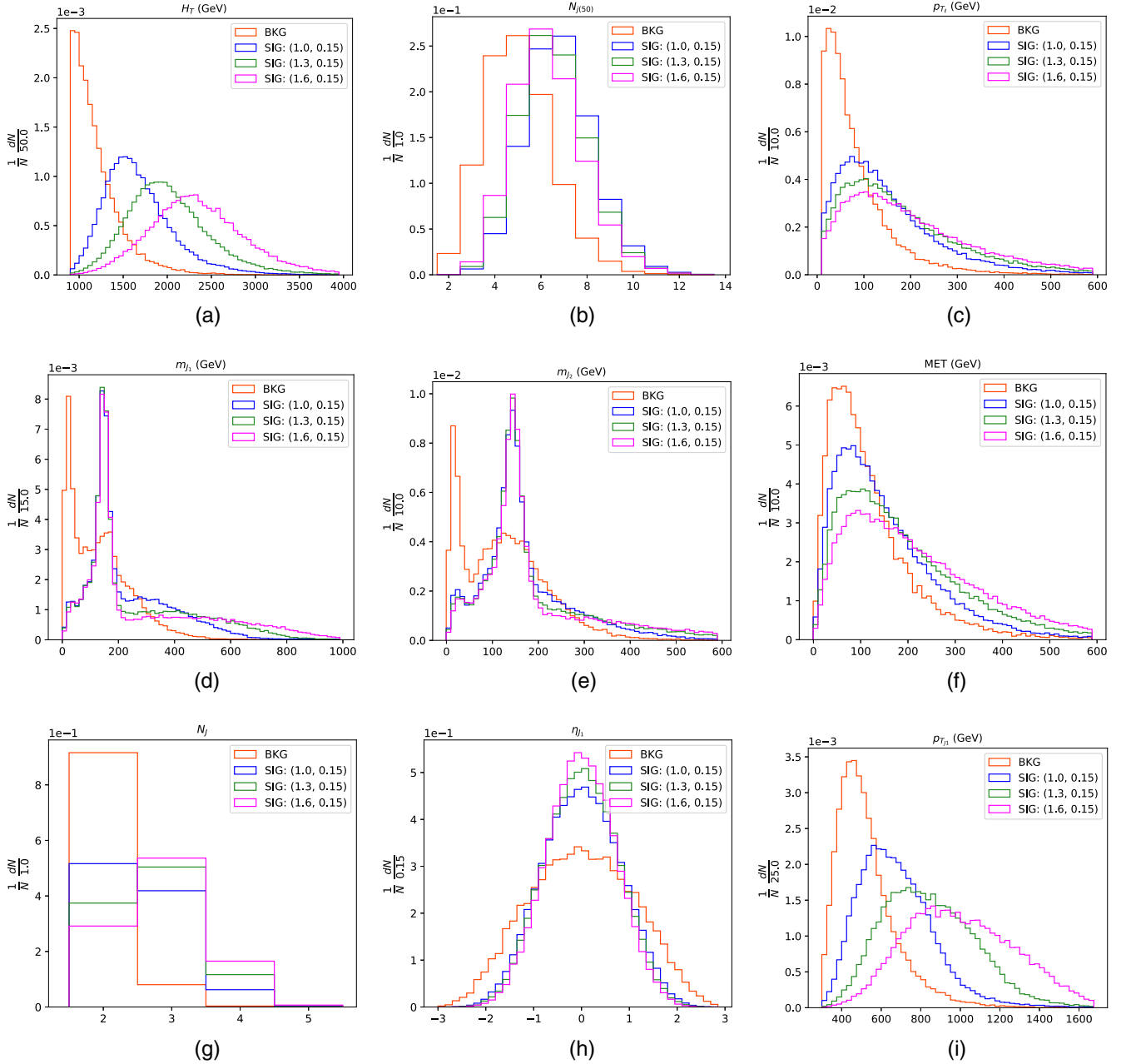


FIG. 6. Normalized input feature distributions for signal and background at a fixed $M_\Phi = 150$ GeV and for three different M_{t_2} points: $M_{t_2} = 1.0, 1.3$ and 1.6 TeV. The background distribution includes all the background processes mentioned in the text.

where N_S and N_B are the number of signal and background events after the optimal cut is applied on the BDT response. For $N_S \ll N_B$, Eq. (10) reduces to

$$\mathcal{Z} = \frac{N_S}{\sqrt{N_S + N_B}}. \quad (11)$$

The above expression is our definition of statistical significance.

We optimize the BDT hyperparameters with the adaptive boosting algorithm [72] at the benchmark mass point:

$(M_{t_2}, M_\Phi) = (1.30 \text{ TeV}, 0.35 \text{ TeV})$ which is roughly in the middle of the mass region considered. We split the dataset into statistically independent subsets for training and testing in a 50–50 ratio. The criteria for optimizing the BDT hyperparameters are (i) Kolmogorov-Smirnov test values between 0.1 and 0.9 for both signal and background, and (ii) a smooth significance curve. A summary of the optimized BDT parameters is given in Table II. In Table III, we show the method-specific and method-unspecific rankings for the optimized BDT hyperparameters at the benchmark point. Defined in Ref. [69], the input features

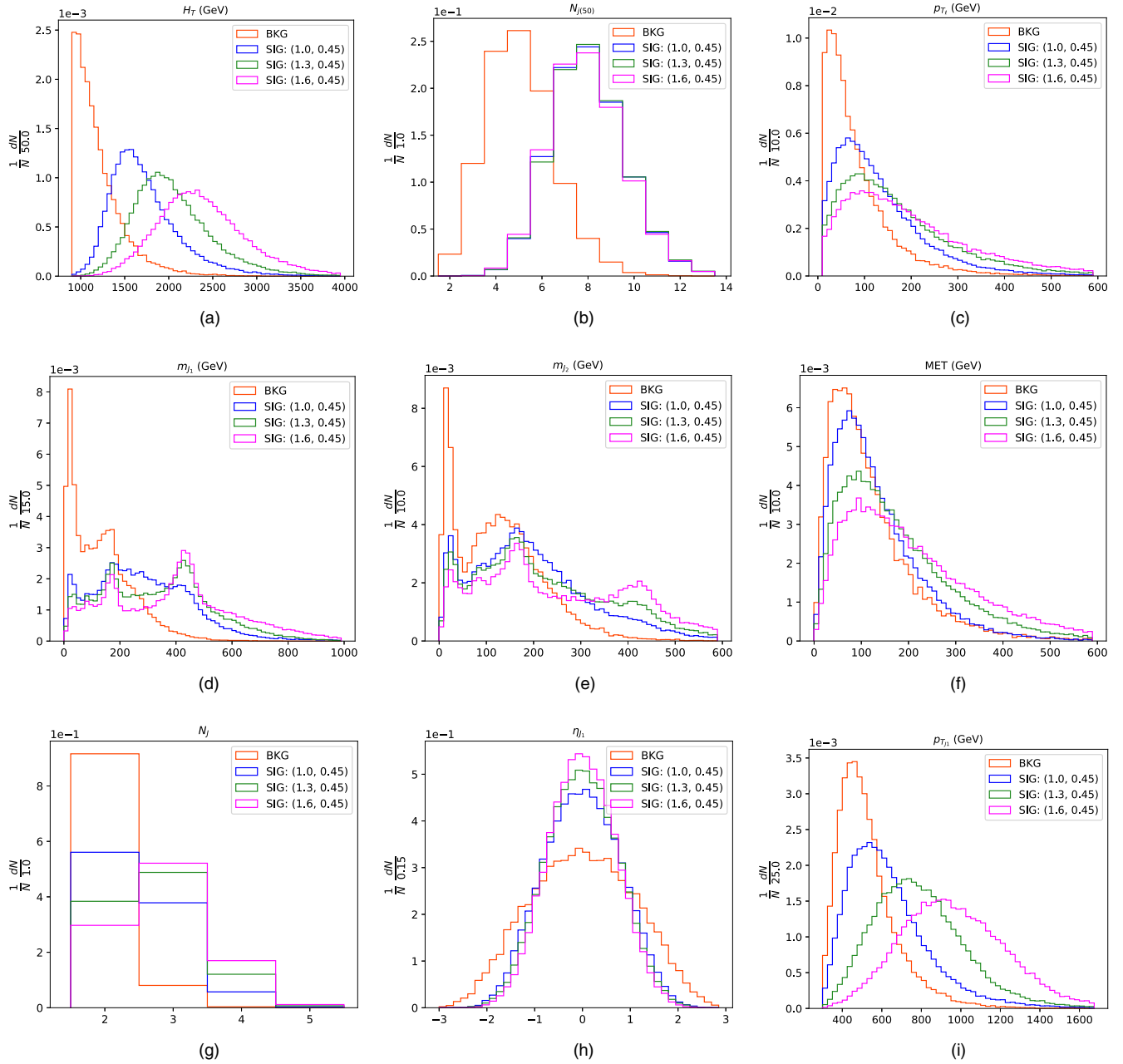


FIG. 7. Normalized input feature distributions for signal and background at a fixed $M_\Phi = 450$ GeV and for three different M_{t_2} points: $M_{t_2} = 1.0, 1.3$ and 1.6 TeV. The background distribution includes all the background processes mentioned in the text.

are ranked by how often they are used to split nodes in decision trees, weighted by the number of events in the node and the separation gain squared achieved at the node (in our case it is the GiniIndex squared).

We use the hyperparameters optimized at the benchmark mass point to obtain the statistical significance \mathcal{Z} with the optimal BDT cut at all mass points. For $M_{t_2} > 1.5$ TeV, where the signal cross sections are low, we use the \mathcal{Z} value obtained for a slightly relaxed cut on the BDT response. We show the BDT response and cut efficiency at the benchmark mass point in Fig. 8. We list \mathcal{Z} at each point in

the mass parameter scan in Fig. 9. We see that, unlike the selection efficiency, the 5σ and 2σ contours follow approximately constant M_{t_2} lines near $M_{t_2} = 1.4$ TeV and $M_{t_2} = 1.7$ TeV, respectively. For a fixed M_{t_2} , the decay products of a heavy Φ are more separated than that of a lighter Φ , so the clustering algorithm is less likely to pick up the entire gg fatjet. Hence, the fatjet features become less separated between the signal and background distributions, leading to a drop in significance. As a result, the gain in the selection efficiency for a heavier Φ [see Fig. 3(a)] is lost to a slight degree in the multivariate analysis (MVA).

TABLE II. Summary of optimized BDT hyperparameters.

BDT parameter	Optimized choice
NTrees	300
MinNodeSize	5.0%
MaxDepth	3
BoostType	AdaBoost
AdaBoostBeta	0.07
UseBaggedBoost	True
BaggedSampleFraction	0.5
SeparationType	GiniIndex
nCuts	50

TABLE III. Summary of method-unspecific and method-specific ranking for the input features at the benchmark mass point.

Feature	Method-unspecific separation	Feature	Method-specific ranking
H_T	0.6689	H_T	0.3606
$p_{T_{J_1}}$	0.4326	$N_{j(50)}$	0.1663
$N_{j(50)}$	0.4241	p_{T_ℓ}	0.1205
m_{J_1}	0.3220	m_{J_1}	0.0923
N_J	0.2913	m_{J_2}	0.0706
p_{T_ℓ}	0.2104	MET	0.0598
m_{J_2}	0.1608	N_J	0.0585
MET	0.1068	η_{J_1}	0.0406
η_{J_1}	0.0722	$p_{T_{J_1}}$	0.0305

E. Inclusive signal

With a MVA optimized for the $\Phi t \bar{t}$ channel with $\beta_{t\Phi} = 1$, we explore the discovery reach for more realistic scenarios where $\text{BR}(T \rightarrow t\Phi) < 1$. Since the signal scales as $\beta_{t\Phi}^2$ in the exclusive mode, its significance drops very fast

with a decreasing $\beta_{t\Phi}$ (see Fig. 10). However, for $\beta_{t\Phi} < 1$, when other t_2 decay modes open up, they can be added to the signal definition. If we consider the mixed mode, i.e., consider

$$pp \rightarrow t_2 \bar{t}_2 \rightarrow (t\Phi)(\bar{t}\Phi/\bar{b}W/\bar{t}Z/\bar{t}h) + \text{c.c.} \quad (12)$$

as our signal, a significant fraction of events from all other decay modes would also pass the selection criteria (Sec. III A) because of their inclusive nature in addition to the $t\Phi$ events. We analyze this case for some representative branching ratios. The mixed mode events generated for $\beta_{t\Phi} < 1$ are passed through the selection cuts and are fed to the optimized MVA. We plot the $3 \text{ ab}^{-1} 5\sigma$ (discovery) and 2σ (exclusion) contours with the three values of $\beta_{t\Phi}$ for both the exclusive and inclusive signals in Fig. 10. We see that the discovery and exclusion reaches in the inclusive mode are significantly higher than those in the exclusive mode. From the figure, we see that a discovery in the exclusive mode is not possible if $\beta_{t\Phi} \leq 0.6$ as the region is excluded by the LHC limits from Fig. 2, whereas for $\beta_{t\Phi} \sim 0.7$, it is possible if $M_\Phi \gtrsim 300 \text{ GeV}$. In the inclusive mode, $\beta_{t\Phi} \sim 0.6$ is the lower limit for a discovery.

F. Single production

We also analyze the single production of t_2 . In the absence of the top quark in the initial state, producing it singly at the LHC is tough. The dominant process is $pp \rightarrow t_2 b j$ through a t -channel W boson exchange. We generate the process and decay the VLQ as $t_2 \rightarrow t\Phi \rightarrow (l\nu b)(gg)$. Since a single production is less phase space suppressed than the pair production, its cross section falls slower than that of the pair production with increasing M_{t_2} . Therefore, one might naively expect the single production to have a better discovery potential in the high VLQ mass region.

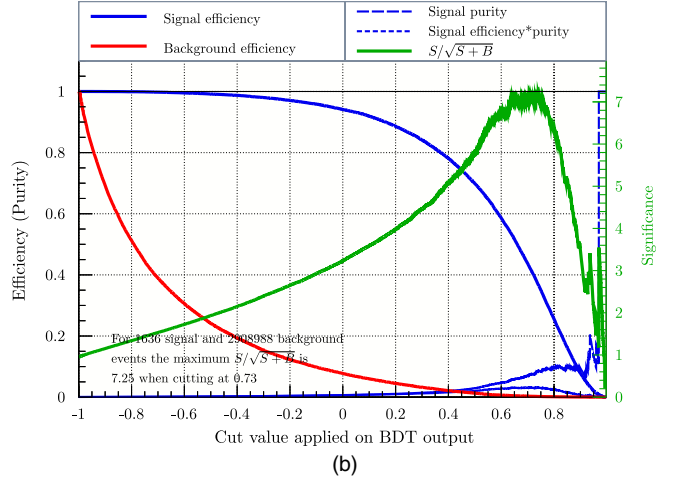
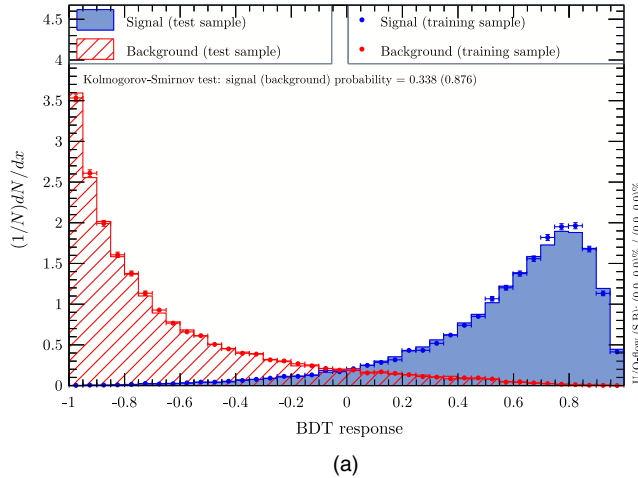


FIG. 8. The BDT response curve and overtraining check are shown in (a) and the cut efficiencies and \mathcal{Z} value at the optimal BDT cut are shown in (b).

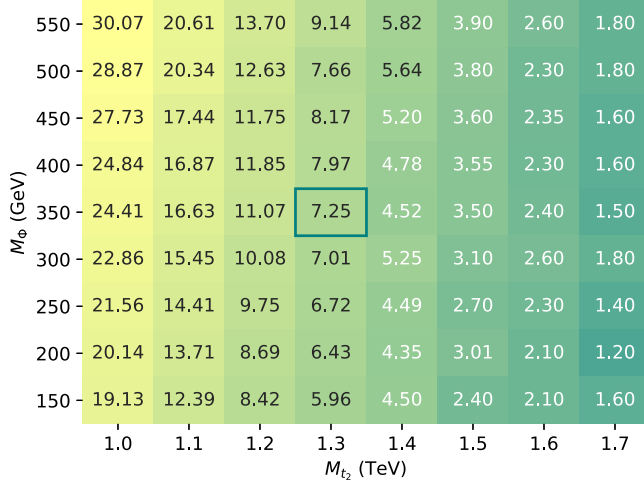


FIG. 9. Statistical significance \mathcal{Z} over the mass range considered. Benchmark mass is highlighted.

However, two factors go against it. There is a competition between the mixing angle θ_L and $\beta_{t\Phi}$ —it is difficult to obtain a large single-production cross section (the $t_2 b W$ coupling goes as $\sin \theta_L$ times the tbW coupling [43]) and a significant BR in the $t_2 \rightarrow t\Phi$ mode simultaneously. Second, the single production signal suffers from a low selection efficiency due to a relatively lower H_T (as a consequence of only one T being present in the process) and the absence of boosted fatjets. The H_T distribution for

single production looks very similar to the background, so its discriminating power is also lower than the $\Phi t\Phi t$ channel. We have tested these by generating the single production signal with $\sin \theta_L \sim 0.1$. Overall, we find that with the t_2 decaying to the singlet Φ , the single production of t_2 is not a promising channel.

IV. SUMMARY AND CONCLUSIONS

In this paper, we have analyzed the pair production of a heavy weak-singlet vectorlike top partner and its subsequent decay into a top quark and a weak-singlet (pseudo)scalar Φ , which gives a dijet signature. In an earlier paper [43], we had shown that the available parameter space in a singlet T model, where the singlet Φ dominantly decays into two gluons, is pretty large and that the collider searches specific to this signature can be used to probe the (M_{t_2}, M_Φ) parameter space effectively. However, the signal for this signature is particularly challenging to isolate from a formidable SM background. We have made use of multivariate analysis techniques, specifically BDTs. We have also utilized jet substructure techniques to tag Φ as a two-prong structure; these features in the signal provided an extra handle to control the SM backgrounds. We optimized the analysis for an ideal scenario where $\text{BR}(t_2 \rightarrow t\Phi) = 1.0$ and $\text{BR}(\Phi \rightarrow gg) = 1.0$ and then presented some realistic cases for the $t_2 \rightarrow t\Phi$ branching which can be probed at the LHC. We have shown the discovery and exclusion prospects for various

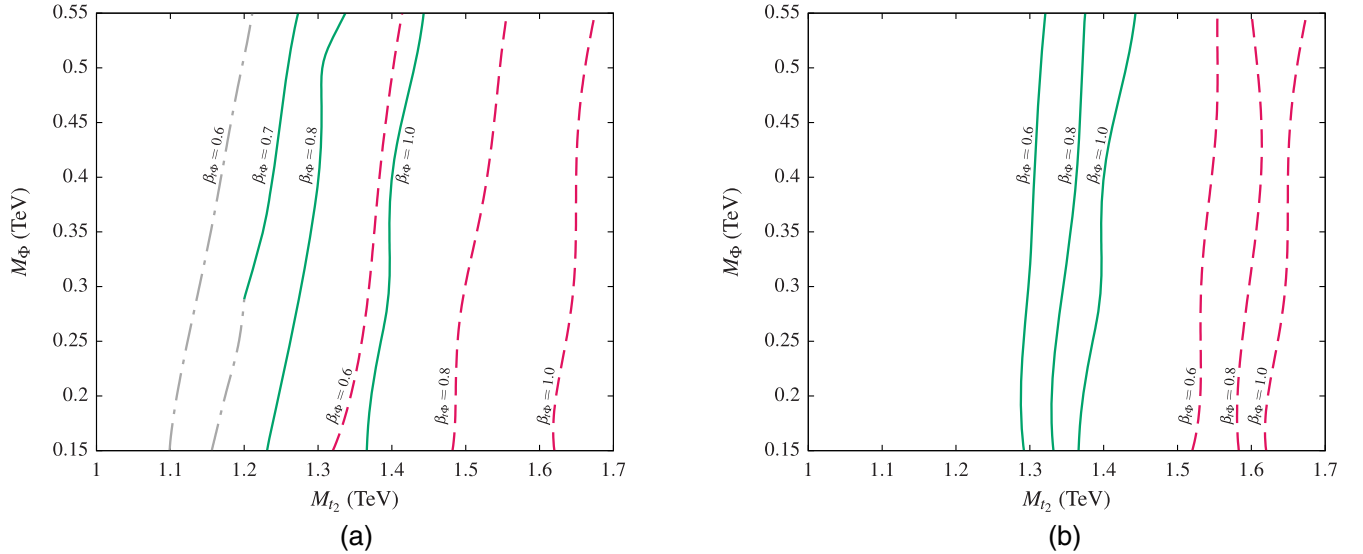


FIG. 10. Discovery reach for $\text{BR}(T \rightarrow t\Phi) \leq 1$ for (a) the exclusive $(t\Phi)(\bar{t}\Phi)$ mode and (b) the inclusive $t\Phi + X$ mode. The 5 σ discovery contours are drawn in green (solid lines) and the 2 σ exclusion contours are in red (dashed lines), marked with the corresponding branching ratios. The parts marked in gray (dot-dashed lines) are excluded by the LHC data as shown in Fig. 2.

combinations of t_2 and Φ masses in both exclusive ($t_2\bar{t}_2 \rightarrow t\Phi\bar{t}\Phi$) as well as inclusive ($t_2\bar{t}_2 \rightarrow t\Phi + X$) modes, where X is any of the standard decay modes of t_2 .

There are other similar extensions to the SM containing heavy top partners in different weak representations (e.g., doublet) with a new decay mode ($t_2 \rightarrow t\Phi$). Since we treat the branching ratios as independent quantities, our search strategy allows for straightforward projection of limits in these models as well. Our study also offers predictive insights into exclusive and inclusive VLQ searches at the LHC.

The UNIVERSAL FeynRules output [73] files used in this paper are available; see [74].

ACKNOWLEDGMENTS

We acknowledge the high-performance computing time at the Padmanabha cluster, India. A. B. is supported by the (Science and Technology Facilities Council) STFC under Grant No. ST/T000945/1. K. B. and C. N. acknowledge Department of Science and Technology (DST)-Inspire for their fellowships.

APPENDIX: LAGRANGIAN AND BENCHMARKS

We reproduce the terms relevant for the top sector mass matrix from Ref. [43] as

$$\mathcal{L} \supset -\{\lambda_t(\bar{Q}_L H_T)t_R + \omega_T(\bar{Q}_L H_T)T_R + M_T\bar{T}_L T_R + \text{H.c.}\},$$

where Q_L is the third-generation left-handed quark doublet and $H_T = i\sigma_2 H^*$, with H being the Higgs doublet. The top Yukawa coupling is denoted by λ_t , ω_T is the off-diagonal coupling and M_T is the vectorlike mass term. After EWSB, we get the mass matrix \mathcal{M} as

$$\mathcal{L}_{\text{mass}} = (\bar{t}_L \quad \bar{T}_L) \begin{pmatrix} \lambda_t \frac{v}{\sqrt{2}} & \omega_T \frac{v}{\sqrt{2}} \\ 0 & M_T \end{pmatrix} \begin{pmatrix} t_R \\ T_R \end{pmatrix} + \text{H.c.},$$

where v is the Higgs vacuum expectation value. The matrix \mathcal{M} can be diagonalized by biorthogonal rotations and the left and right mixing angles are given by

$$\tan(2\theta_L) = \frac{2M_T\mu_1}{m_t^2 + \mu_1^2 - M_T^2},$$

$$\tan(2\theta_R) = \frac{2m_t\mu_1}{m_t^2 - M_T^2 - \mu_1^2},$$

where $m_t = \lambda_t \frac{v}{\sqrt{2}}$ and $\mu_1 = \omega_T \frac{v}{\sqrt{2}}$. The mass eigenvalues m_{t_1} and M_{t_2} are

$$m_{t_1}^2, M_{t_2}^2 = \frac{1}{2} \left[(m_t^2 + \mu_1^2 + M_T^2) \mp \sqrt{(m_t^2 + \mu_1^2 + M_T^2)^2 - 4m_t^2 M_T^2} \right].$$

Expressions for the partial decay widths of t_2 and Φ are found in Ref. [43]. With those expressions, one can obtain the BRs of these particles. The BR plots for some benchmark points are shown in Figs. 11(a)–11(f) and relate to the benchmarks presented in Ref. [43] for the singlet T model with a scalar ϕ . Figures 11(g) and 11(h) show the behavior of the benchmark point $\{M_{t_2}, M_\phi\} = \{1.3, 0.35\}$ TeV for which the analysis is optimized. All of the plots show scenarios in which the $t_2 \rightarrow t\Phi$ mode dominates. From the exclusion plot in Fig. 2, we see that only beyond $M_{t_2} = 1.3$ TeV, the standard decays of t_2 can dominate, i.e., $\text{BR}(t_2 \rightarrow t\phi) \lesssim 0.5$. For example, we get $\text{BR}(t_2 \rightarrow t\phi) \approx 0.5$ for $M_{t_2} = 1.3$ TeV, $\lambda_\phi^a \approx 0.26$, $\lambda_\phi^b \approx 0.1$, $\mu_1 \approx 10$ GeV and $M_\phi \approx 350$ GeV. Hence, if the couplings are smaller for the same mass parameters (or if μ_1 is bigger with the other parameters held fixed), the standard decays of the singlet top partner will dominate over the new mode.

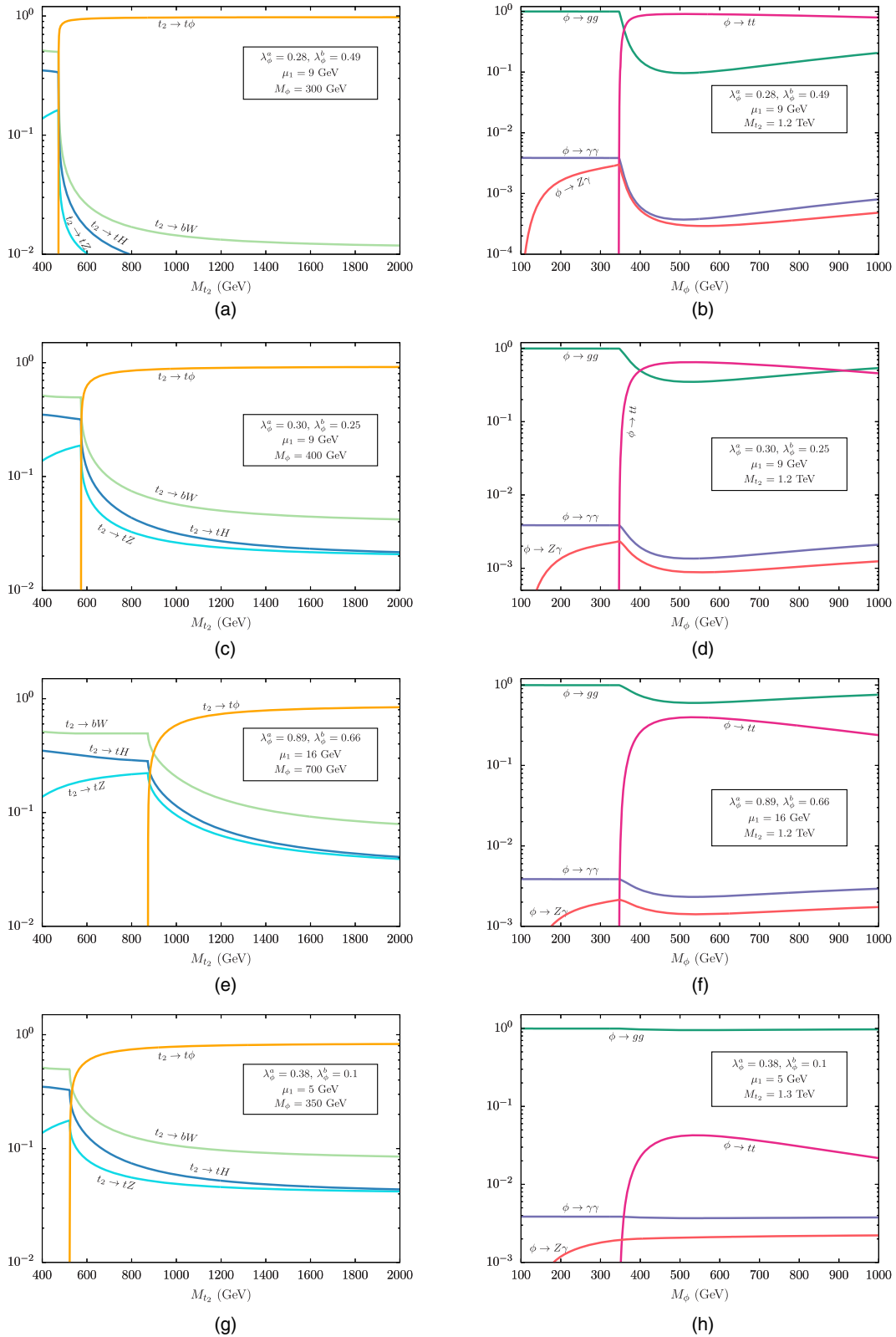


FIG. 11. Illustrative BR plots for t_2 and Φ decays. Panels (a)–(f) relate to the benchmark parameters identified in Ref. [43] for the singlet T model. Panels (g) and (h) correspond to the parameters we have used to optimize the analysis in this paper.

- [1] D. B. Kaplan and H. Georgi, $SU(2) \times U(1)$ breaking by vacuum misalignment, *Phys. Lett.* **136B**, 183 (1984).
- [2] D. B. Kaplan, Flavor at SSC energies: A new mechanism for dynamically generated fermion masses, *Nucl. Phys.* **B365**, 259 (1991).
- [3] K. Agashe, R. Contino, and A. Pomarol, The minimal composite Higgs model, *Nucl. Phys.* **B719**, 165 (2005).
- [4] G. Ferretti and D. Karateev, Fermionic UV completions of composite Higgs models, *J. High Energy Phys.* **03** (2014) 077.
- [5] G. Ferretti, UV completions of partial compositeness: The case for a $SU(4)$ gauge group, *J. High Energy Phys.* **06** (2014) 142.
- [6] G. Ferretti, Gauge theories of partial compositeness: Scenarios for run-II of the LHC, *J. High Energy Phys.* **06** (2016) 107.
- [7] A. Banerjee, D. B. Franzosi, and G. Ferretti, Modeling vectorlike quarks in partial compositeness framework, *J. High Energy Phys.* **03** (2022) 200.
- [8] S. Chang, J. Hisano, H. Nakano, N. Okada, and M. Yamaguchi, Bulk standard model in the Randall-Sundrum background, *Phys. Rev. D* **62**, 084025 (2000).
- [9] T. Gherghetta and A. Pomarol, Bulk fields and supersymmetry in a slice of AdS, *Nucl. Phys.* **B586**, 141 (2000).
- [10] R. Contino, Y. Nomura, and A. Pomarol, Higgs as a holographic pseudo-Goldstone boson, *Nucl. Phys.* **B671**, 148 (2003).
- [11] S. Gopalakrishna, T. Mandal, S. Mitra, and R. Tibrewala, LHC signatures of a vectorlike b' , *Phys. Rev. D* **84**, 055001 (2011).
- [12] S. Gopalakrishna, T. Mandal, S. Mitra, and G. Moreau, LHC signatures of warped-space vectorlike quarks, *J. High Energy Phys.* **08** (2014) 079.
- [13] R. Barceló, S. Mitra, and G. Moreau, On a boundary-localized Higgs boson in 5D theories, *Eur. Phys. J. C* **75**, 527 (2015).
- [14] N. Arkani-Hamed, A. G. Cohen, E. Katz, A. E. Nelson, T. Gregoire, and J. G. Wacker, The minimal moose for a Little Higgs, *J. High Energy Phys.* **08** (2002) 021.
- [15] M. Schmaltz, Physics beyond the standard model (theory): Introducing the Little Higgs, *Nucl. Phys. B, Proc. Suppl.* **117**, 40 (2003).
- [16] M. Perelstein, M. E. Peskin, and A. Pierce, Top quarks and electroweak symmetry breaking in Little Higgs models, *Phys. Rev. D* **69**, 075002 (2004).
- [17] S. P. Martin, Extra vectorlike matter and the lightest Higgs scalar boson mass in low-energy supersymmetry, *Phys. Rev. D* **81**, 035004 (2010).
- [18] S. Gopalakrishna, T. S. Mukherjee, and S. Sadhukhan, Extra neutral scalars with vectorlike fermions at the LHC, *Phys. Rev. D* **93**, 055004 (2016).
- [19] J. Serra, Beyond the minimal top partner decay, *J. High Energy Phys.* **09** (2015) 176.
- [20] A. Anandakrishnan, J. H. Collins, M. Farina, E. Kuflik, and M. Perelstein, Odd top partners at the LHC, *Phys. Rev. D* **93**, 075009 (2016).
- [21] S. Banerjee, D. Barducci, G. Bélanger, and C. Delaunay, Implications of a high-mass diphoton resonance for heavy quark searches, *J. High Energy Phys.* **11** (2016) 154.
- [22] S. Kraml, U. Laa, L. Panizzi, and H. Prager, Scalar versus fermionic top partner interpretations of $t\bar{t} + E_T^{\text{miss}}$ searches at the LHC, *J. High Energy Phys.* **11** (2016) 107.
- [23] B. A. Dobrescu and F. Yu, Exotic signals of vectorlike quarks, *J. Phys. G* **45**, 08LT01 (2018).
- [24] J. A. Aguilar-Saavedra, D. E. López-Fogliani, and C. Muñoz, Novel signatures for vectorlike quarks, *J. High Energy Phys.* **06** (2017) 095.
- [25] M. Chala, Direct bounds on heavy toplike quarks with standard and exotic decays, *Phys. Rev. D* **96**, 015028 (2017).
- [26] S. Moretti, D. O'Brien, L. Panizzi, and H. Prager, Production of extra quarks decaying to dark matter beyond the narrow width approximation at the LHC, *Phys. Rev. D* **96**, 035033 (2017).
- [27] N. Bizot, G. Cacciapaglia, and T. Flacke, Common exotic decays of top partners, *J. High Energy Phys.* **06** (2018) 065.
- [28] S. Colucci, B. Fuks, F. Giacchino, L. Lopez Honorez, M. H. G. Tytgat, and J. Vandecasteele, Top-philic vectorlike portal to scalar dark matter, *Phys. Rev. D* **98**, 035002 (2018).
- [29] H. Han, L. Huang, T. Ma, J. Shu, T. M. P. Tait, and Y. Wu, Six top messages of new physics at the LHC, *J. High Energy Phys.* **10** (2019) 008.
- [30] R. Dermisek, E. Lunghi, and S. Shin, Hunting for vectorlike quarks, *J. High Energy Phys.* **04** (2019) 019; Erratum, *J. High Energy Phys.* **10** (2020) 058.
- [31] J. H. Kim, S. D. Lane, H.-S. Lee, I. M. Lewis, and M. Sullivan, Searching for dark photons with Maverick top partners, *Phys. Rev. D* **101**, 035041 (2020).
- [32] K.-P. Xie, G. Cacciapaglia, and T. Flacke, Exotic decays of top partners with charge 5/3: Bounds and opportunities, *J. High Energy Phys.* **10** (2019) 134.
- [33] R. Benbrik *et al.*, Signatures of vectorlike top partners decaying into new neutral scalar or pseudoscalar bosons, *J. High Energy Phys.* **05** (2020) 028.
- [34] G. Cacciapaglia, T. Flacke, M. Park, and M. Zhang, Exotic decays of top partners: Mind the search gap, *Phys. Lett. B* **798**, 135015 (2019).
- [35] R. Dermisek, E. Lunghi, N. McGinnis, and S. Shin, Signals with six bottom quarks for charged and neutral Higgs bosons, *J. High Energy Phys.* **07** (2020) 241.
- [36] D. Wang, L. Wu, and M. Zhang, Hunting for top partner with a new signature at the LHC, *Phys. Rev. D* **103**, 115017 (2021).
- [37] D. Das, B. De, and S. Mitra, Cancellation in dark matter-nucleon interactions: The role of nonstandard-modellike Yukawa couplings, *Phys. Lett. B* **815**, 136159 (2021).
- [38] D. Choudhury, K. Deka, and N. Kumar, Looking for a vectorlike B quark at the LHC using jet substructure, *Phys. Rev. D* **104**, 035004 (2021).
- [39] R. Dermisek, E. Lunghi, N. McGinnis, and S. Shin, Tau-jet signatures of vectorlike quark decays to heavy charged and neutral Higgs bosons, *J. High Energy Phys.* **08** (2021) 159.
- [40] G. Corcella, A. Costantini, M. Ghezzi, L. Panizzi, G. M. Pruna, and J. Šalko, Vectorlike quarks decaying into singly and doubly charged bosons at LHC, *J. High Energy Phys.* **10** (2021) 108.
- [41] S. Dasgupta, R. Pramanick, and T. S. Ray, Broad toplike vector quarks at LHC and HL-LHC, *Phys. Rev. D* **105**, 035032 (2022).

- [42] J. M. Cline, A. Friedlander, D.-M. He, K. Kainulainen, B. Laurent, and D. Tucker-Smith, Baryogenesis and gravity waves from a UV-completed electroweak phase transition, *Phys. Rev. D* **103**, 123529 (2021).
- [43] A. Bhardwaj, T. Mandal, S. Mitra, and C. Neeraj, Roadmap to explore vectorlike quarks decaying to a new scalar or pseudoscalar, [arXiv:2203.13753](https://arxiv.org/abs/2203.13753).
- [44] A. M. Sirunyan *et al.* (CMS Collaboration), Search for pair production of vectorlike quarks in the fully hadronic final state, *Phys. Rev. D* **100**, 072001 (2019).
- [45] ATLAS Collaboration, Search for pair-production of vectorlike quarks in pp collision events at $\sqrt{s} = 13$ TeV with at least one leptonically-decaying Z boson and a third-generation quark with the ATLAS detector, <https://cds.cern.ch/record/2773300>.
- [46] G. Aad *et al.* (ATLAS Collaboration), Search for single production of a vectorlike T quark decaying into a Higgs boson and top quark with fully hadronic final states using the ATLAS detector, *Phys. Rev. D* **105**, 092012 (2022).
- [47] ATLAS Collaboration, Search for single production of vectorlike T quarks decaying to Ht or Zt in pp collisions at $\sqrt{s} = 13$ TeV with the ATLAS detector, Technical Report No. ATLAS-CONF-2021-040, 2021.
- [48] A. M. Sirunyan *et al.* (CMS Collaboration), A search for bottom-type, vectorlike quark pair production in a fully hadronic final state in proton-proton collisions at $\sqrt{s} = 13$ TeV, *Phys. Rev. D* **102**, 112004 (2020).
- [49] G. Aad *et al.* (ATLAS Collaboration), Search for resonances decaying into photon pairs in 139 fb^{-1} of pp collisions at $s = 13$ TeV with the ATLAS detector, *Phys. Lett. B* **822**, 136651 (2021).
- [50] J. Alwall, R. Frederix, S. Frixione, V. Hirschi, F. Maltoni, O. Mattelaer, H.-S. Shao, T. Stelzer, P. Torrielli, and M. Zaro, The automated computation of tree-level and next-to-leading order differential cross sections, and their matching to parton shower simulations, *J. High Energy Phys.* **07** (2014) 079.
- [51] J. Pumplin, D. R. Stump, J. Huston, H. L. Lai, P. M. Nadolsky, and W. K. Tung, New generation of parton distributions with uncertainties from global QCD analysis, *J. High Energy Phys.* **07** (2002) 012.
- [52] T. Sjöstrand, S. Ask, J. R. Christiansen, R. Corke, N. Desai, P. Ilten, S. Mrenna, S. Prestel, C. O. Rasmussen, and P. Z. Skands, An introduction to PYTHIA 8.2, *Comput. Phys. Commun.* **191**, 159 (2015).
- [53] J. de Favereau, C. Delaere, P. Demin, A. Giammanco, V. Lemaître, A. Mertens, and M. Selvaggi (DELPHES 3 Collaboration), DELPHES 3, A modular framework for fast simulation of a generic collider experiment, *J. High Energy Phys.* **02** (2014) 057.
- [54] M. Cacciari, G. P. Salam, and G. Soyez, The anti- k_r jet clustering algorithm, *J. High Energy Phys.* **04** (2008) 063.
- [55] M. Cacciari, G. P. Salam, and G. Soyez, FastJet user manual, *Eur. Phys. J. C* **72**, 1896 (2012).
- [56] M. Aliev, H. Lacker, U. Langenfeld, S. Moch, P. Uwer, and M. Wiedermann, HATHOR: Hadronic top and heavy quarks cross section calculator, *Comput. Phys. Commun.* **182**, 1034 (2011).
- [57] S. Chatrchyan *et al.* (CMS Collaboration), Identification of b -quark jets with the CMS experiment, *J. Instrum.* **8**, P04013 (2013).
- [58] A. M. Sirunyan *et al.* (CMS Collaboration), Identification of heavy-flavour jets with the CMS detector in pp collisions at 13 TeV, *J. Instrum.* **13**, P05011 (2018).
- [59] Y. L. Dokshitzer, G. D. Leder, S. Moretti, and B. R. Webber, Better jet clustering algorithms, *J. High Energy Phys.* **08** (1997) 001.
- [60] A. J. Larkoski, S. Marzani, G. Soyez, and J. Thaler, Soft drop, *J. High Energy Phys.* **05** (2014) 146.
- [61] M. L. Mangano, M. Moretti, F. Piccinini, and M. Treccani, Matching matrix elements and shower evolution for top-quark production in hadronic collisions, *J. High Energy Phys.* **01** (2007) 013.
- [62] C. Muselli, M. Bonvini, S. Forte, S. Marzani, and G. Ridolfi, Top quark pair production beyond NNLO, *J. High Energy Phys.* **08** (2015) 076.
- [63] G. Balossini, G. Montagna, C. M. Carloni Calame, M. Moretti, O. Nicosini, F. Piccinini, M. Treccani, and A. Vicini, Combination of electroweak and QCD corrections to single W production at the Fermilab Tevatron and the CERN LHC, *J. High Energy Phys.* **01** (2010) 013.
- [64] N. Kidonakis, Theoretical results for electroweak-boson and single-top production, *Proc. Sci.*, DIS2015 (2015) 170 [[arXiv:1506.04072](https://arxiv.org/abs/1506.04072)].
- [65] A. Broggio, A. Ferroglia, R. Frederix, D. Pagani, B. D. Pecjak, and I. Tsinikos, Top-quark pair hadroproduction in association with a heavy boson at NLO + NNLL including EW corrections, *J. High Energy Phys.* **08** (2019) 039.
- [66] S. Dittmaier *et al.* (LHC Higgs Cross Section Working Group Collaboration), *Handbook of LHC Higgs Cross Sections: 1. Inclusive Observables* (CERN, Geneva, 2011).
- [67] J. Thaler and K. Van Tilburg, Identifying boosted objects with n -subjettiness, *J. High Energy Phys.* **03** (2011) 015.
- [68] A. J. Larkoski, G. P. Salam, and J. Thaler, Energy correlation functions for jet substructure, *J. High Energy Phys.* **06** (2013) 108.
- [69] A. Hocker *et al.*, TMVA—Toolkit for multivariate data analysis, [arXiv:physics/0703039](https://arxiv.org/abs/physics/0703039).
- [70] CMS Collaboration, Performance of quark/gluon discrimination in 8 TeV pp data, Technical Report No. CMS-PAS-JME-13-002, CERN, Geneva, 2013, <https://cds.cern.ch/record/1599732>.
- [71] C. K. Khosa and S. Marzani, Higgs boson tagging with the Lund jet plane, *Phys. Rev. D* **104**, 055043 (2021).
- [72] Y. Freund and R. E. Schapire, A decision-theoretic generalization of on-line learning and an application to boosting, *J. Comput. Syst. Sci.* **55**, 119 (1997).
- [73] C. Degrande, C. Duhr, B. Fuks, D. Grellscheid, O. Mattelaer, and T. Reiter, UFO—The Universal FeynRules Output, *Comput. Phys. Commun.* **183**, 1201 (2012).
- [74] See <https://github.com/rsrchtsm/vectorlikequarks/> under the name SingTplusPhi.